Supporting Information

Pyrene-based red-emitting aggregation-induced emission luminogens: from high-efficiency structural construction to anti-counterfeiting applications

Hua-Long Li,‡ Zeng-Min Xue,‡ Guang Yang, Fei Meng, Hong-Tao Lin, Wen-Xuan Zhao,* Shu-Hai Chen,* Chuan-Zeng Wang*

Contents

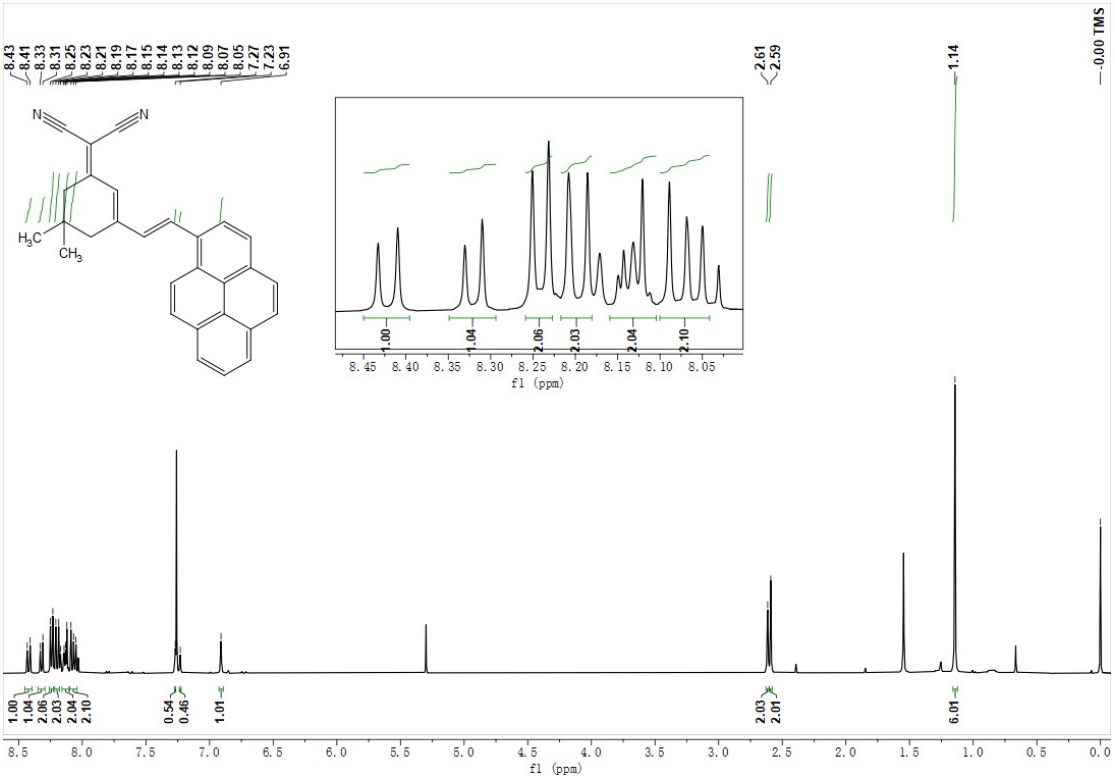

Figure S1. ^{1}H NMR spectrum of **DCI-Py-1** (400 MHz, 293 K, $CDCl_3$)

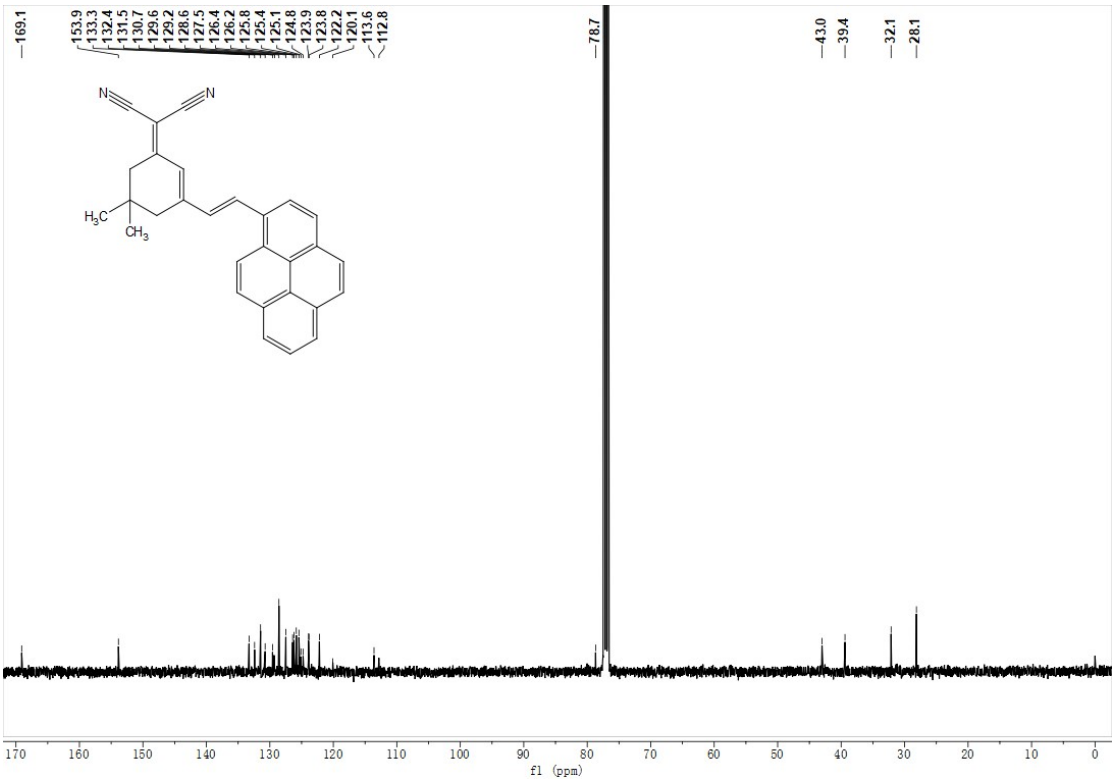

Figure S2. ^{13}C NMR spectrum of **DCI-Py-1** (101 MHz, 293 K, $CDCl_3$)

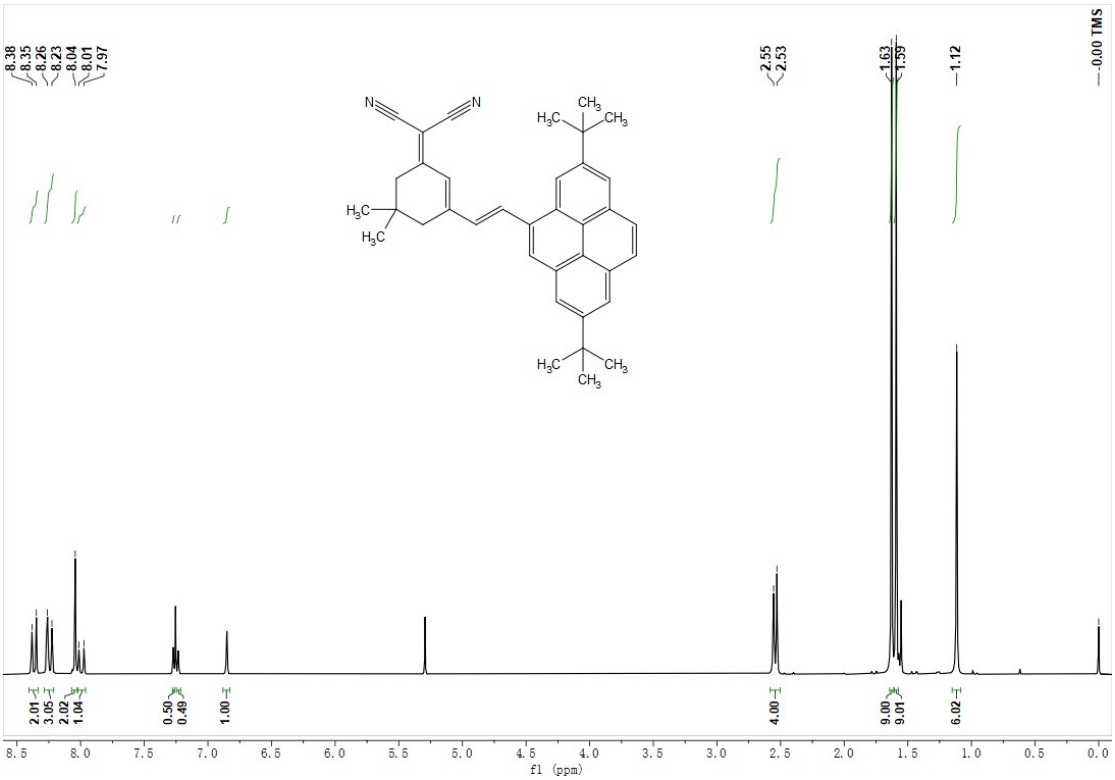

Figure S3. ^{1}H NMR spectrum of **DCI-Py-2** (400 MHz, 293 K, $CDCl_3$)

Figure S4. ^{13}C NMR spectrum of **DCI-Py-2** (101 MHz, 293 K, $CDCl_3$)

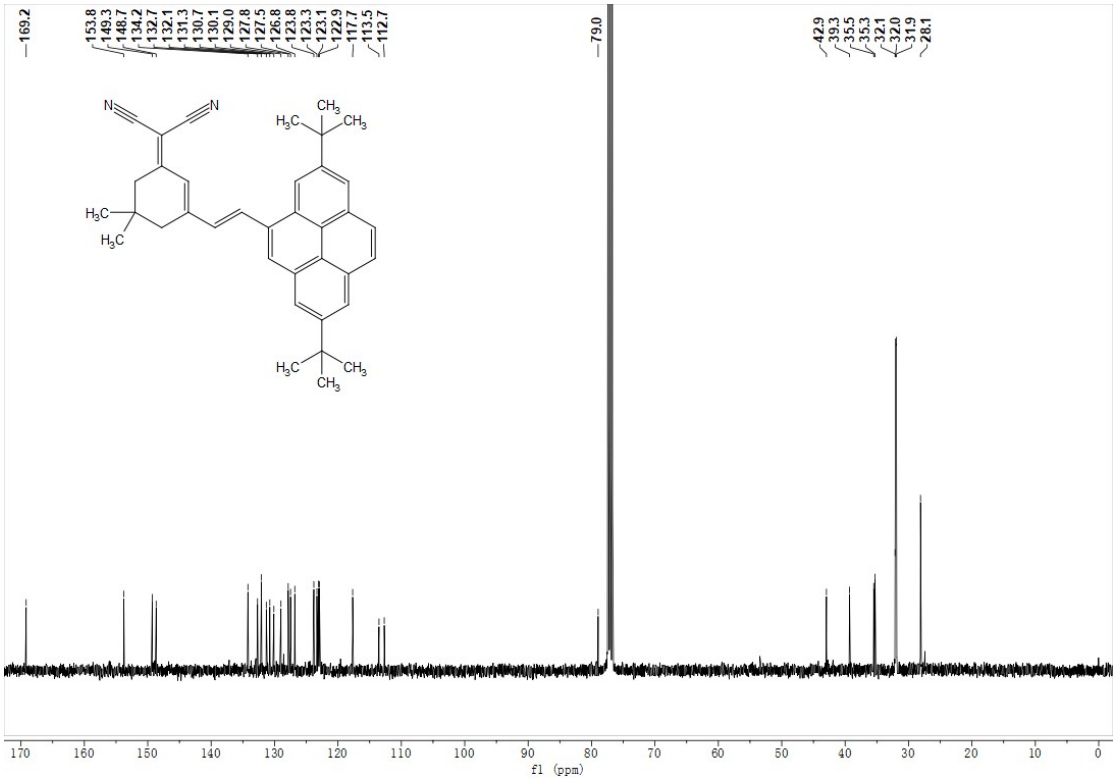

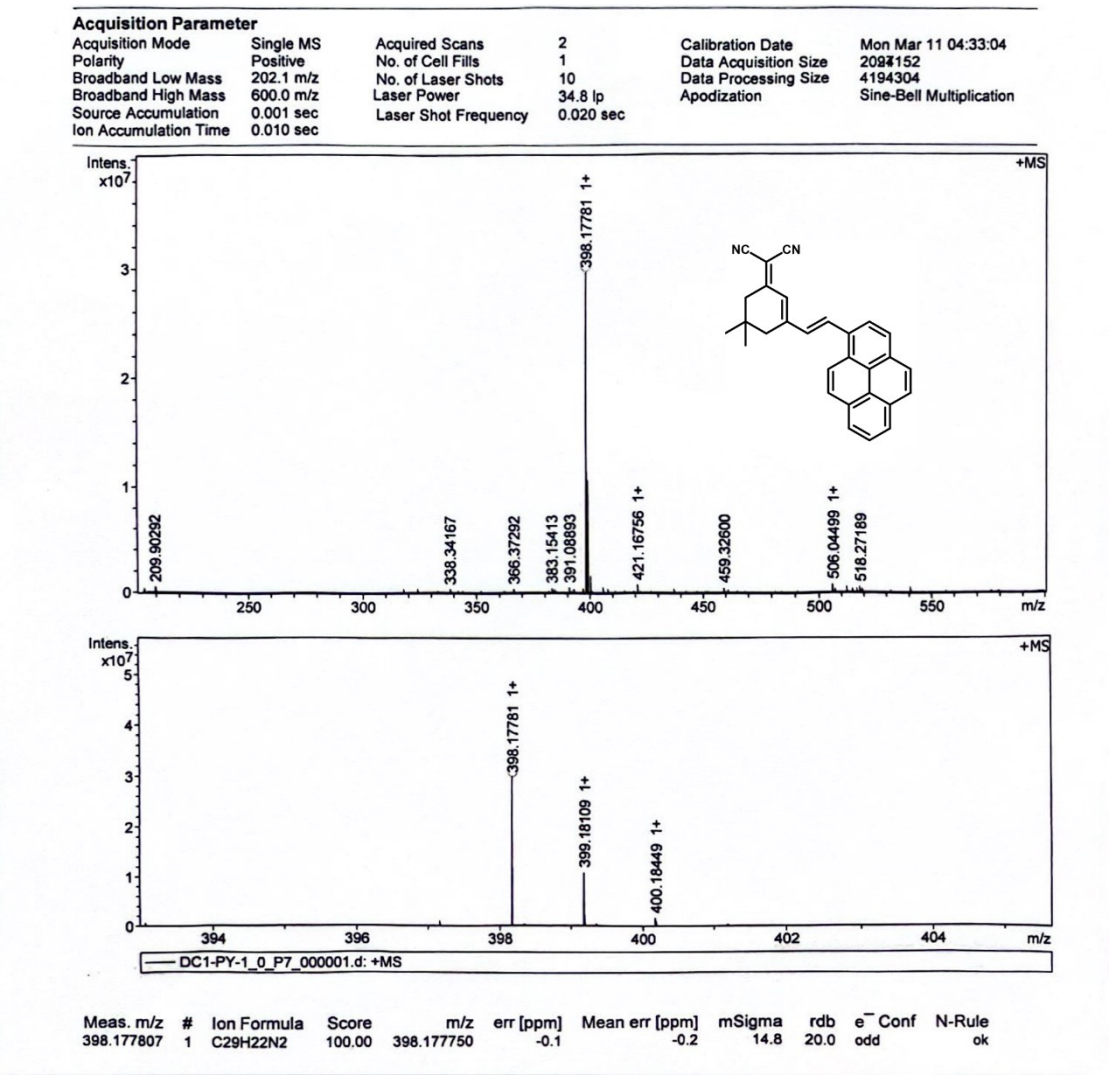

Figure S5. MALDI-FTICR-MS of spectra of **DCI-Py-1**

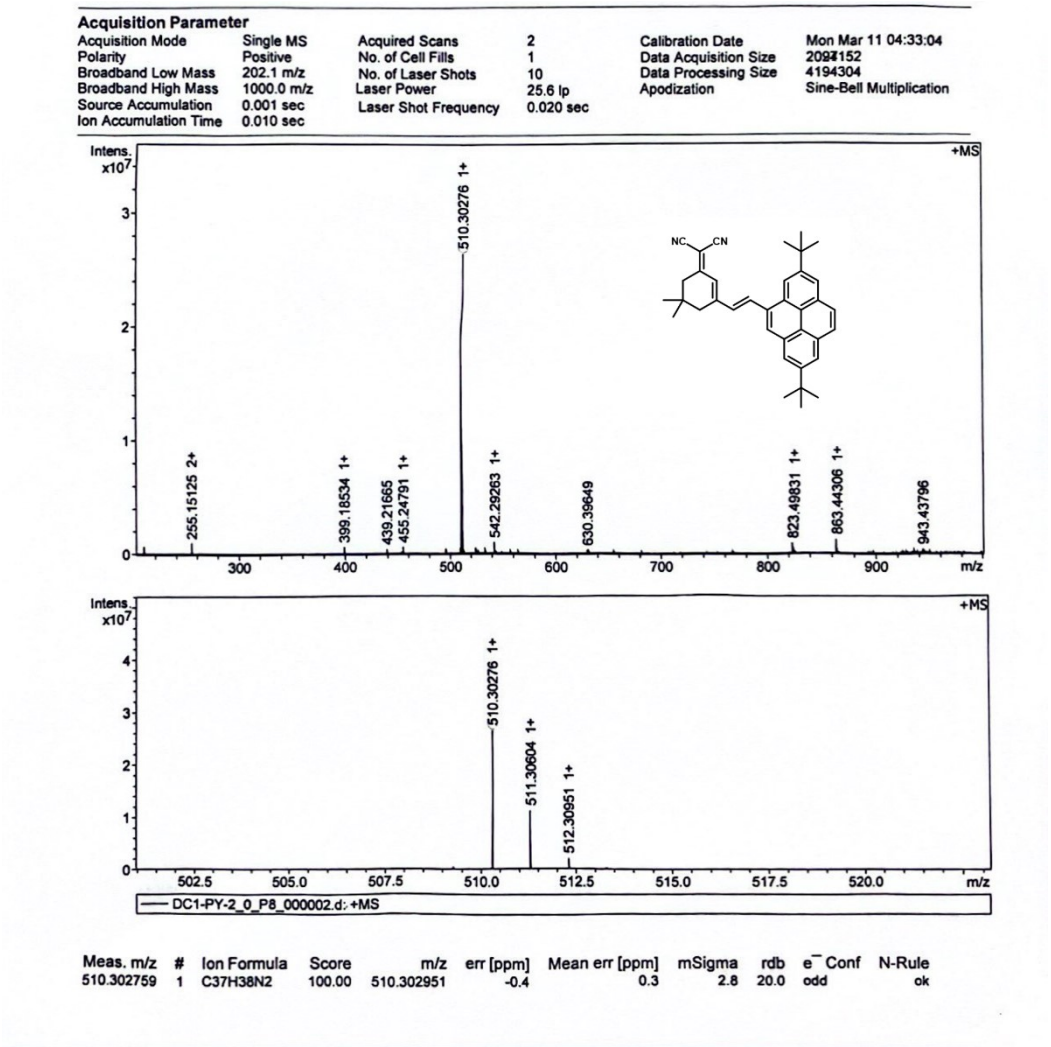

Figure S6. MALDI-FTICR-MS of spectra of **DCI-Py-2**

Table S1. Crystal data and structure refinement of **DCI-Py-1** and **DCI-Py-2**. [a, b]

Compounds	**DCI-Py-1**	**DCI-Py-2**
Empirical formula	$C_{30}H_{24}Cl_2N_2$	$C_{37}H_{38}N_2$
Formula weight	483.41	510.69
Crystal system	triclinic	orthorhombic
Space group	*P-1*	*P n a 21*
a[Å]	9.2959(6)	13.2805(13)
b[Å]	9.4991(5)	35.882(9)
c[Å]	15.3763(9)	6.2204(9)
α[°]	97.995(5)	90
β[°]	95.595(5)	90
γ[°]	112.544(6)	90
Volume[Å^3]	1224.82(14)	2964.2(9)
Z	2	4
μ	2.537 mm^{-1}	0.499
F(000)	504	1096
Crystal size[mm^3]	0.32 × 0.08 × 0.01	0.38 × 0.02 × 0.01
Dcalcd[Mg/m^3]	1.311	1.144
Temperature [K]	170(10)	170(10)
Measured reflns	4943	5537
Unique reflns	4214	4376
Parameters	310	392
R(int)	0.1363	0.1197
$R[I> 2\sigma(I)]$[a]	0.1289	0.0983
*wR*2[all data][b]	0.3405	0.2330

[a]$R_1 = \sum||F_o|-|F_c|| / \sum|F_o|$ (based on reflections with $F_o^2>2\sigma F^2$) [b]$wR_2 = [\sum[w(F_o^2-F_c^2)^2]/\sum[w(F_o^2)^2]]^{1/2}$; $w=1/[\sigma^2(F_o^2) + (0.095P)^2]$; $P = [\max(F_o^2, 0) + 2F_c^2]/3$(also with $F_o^2>2\sigma F^2$)

Table S2. The energy level diagrams of **DCI-Py-1** and **DCI-Py-2**.

Compounds	DFT (eV)		
	HOMO	LUMO	ΔE_g
DCI-Py-1	-5.51	-2.92	2.59
DCI-Py-2	-5.49	-2.84	2.65

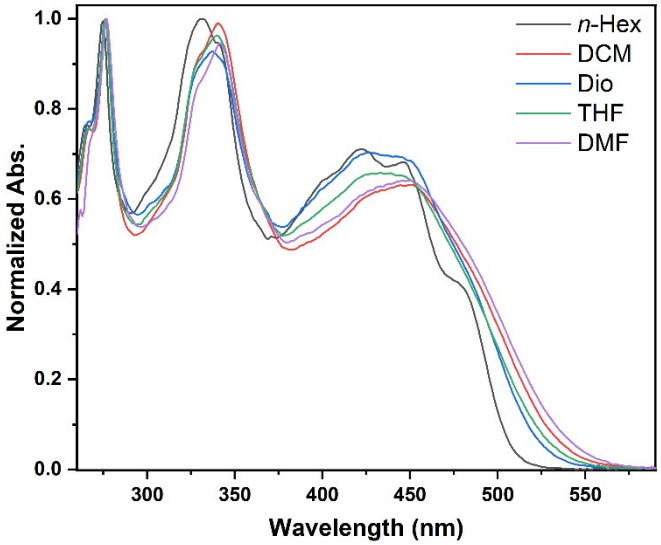

Figure S7. Solvatochromism effect of absorption spectra for **DCI-Py-1** in *n*-Hexane, DCM, 1,4-Dioxane, THF, and DMF, respectively.

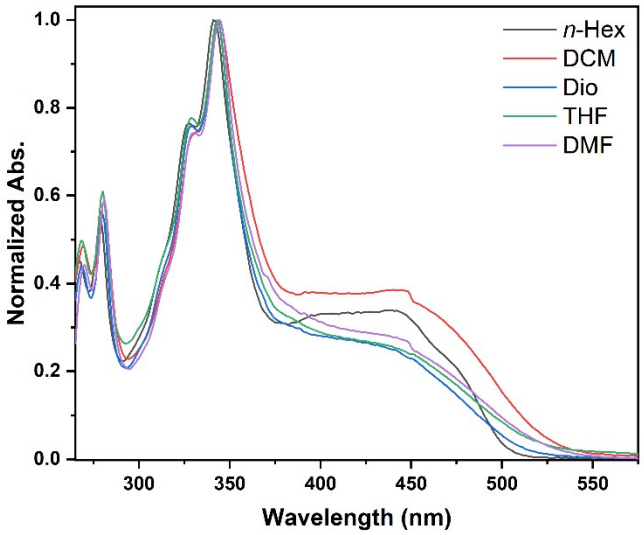

Figure S8. Solvatochromism effect of absorption spectra for **DCI-Py-2** in *n*-Hexane, DCM, 1,4-Dioxane, THF, and DMF, respectively.

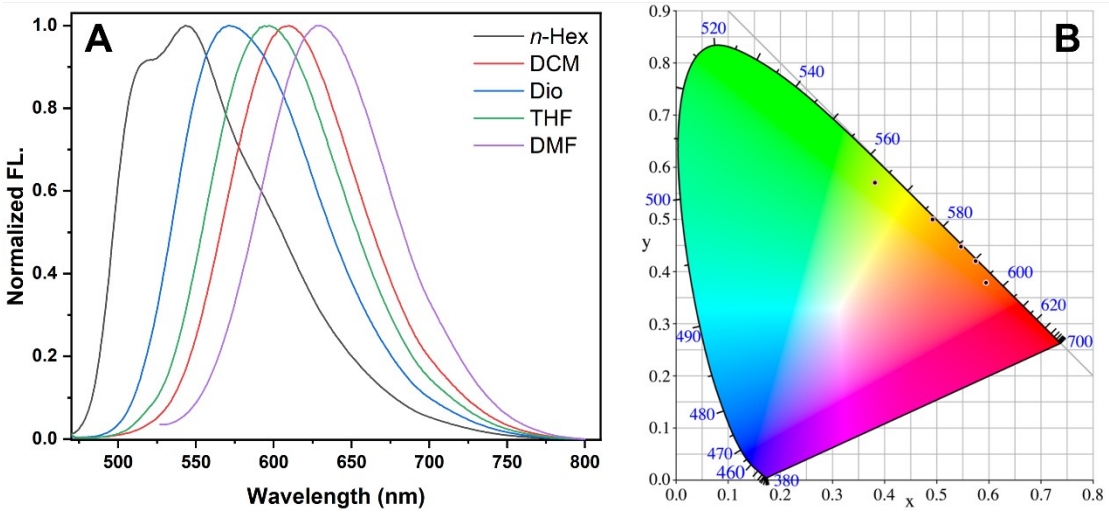

Figure S9. (A) Solvatochromism effect of emission spectra for **DCI-Py-1** in *n*-Hexane, DCM, 1,4-Dioxane, THF, and DMF, respectively. (B) CIE 1931 chromaticity diagram

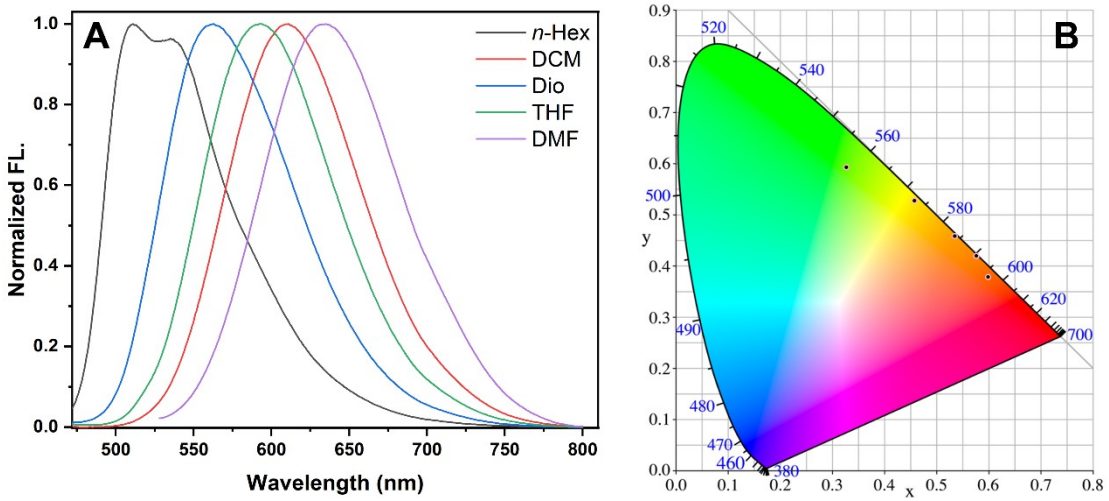

Figure S10. (A) Solvatochromism effect of emission spectra for **DCI-Py-2** in *n*-Hexane, DCM, 1,4-Dioxane, THF, and DMF, respectively. (B) CIE 1931 chromaticity diagram.

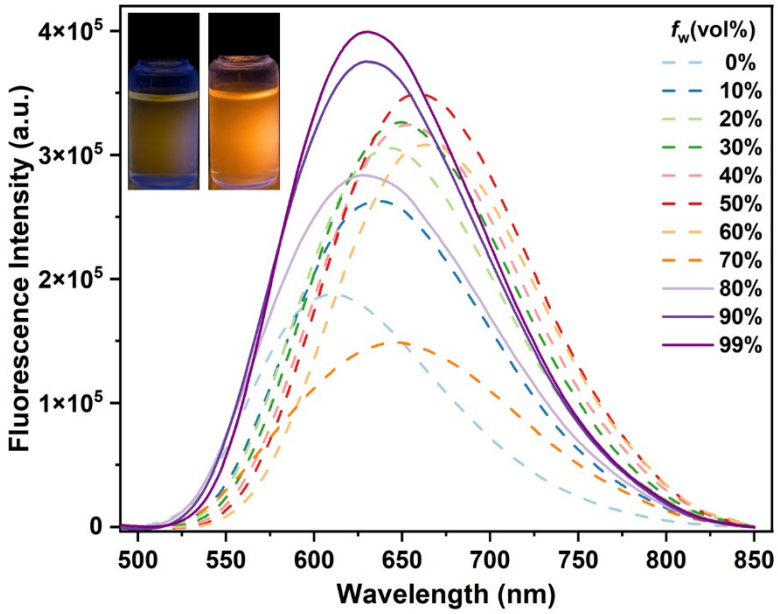

Figure S11. PL spectra of **DCI-Py-2** in THF/water mixtures with different water fractions (f_w).

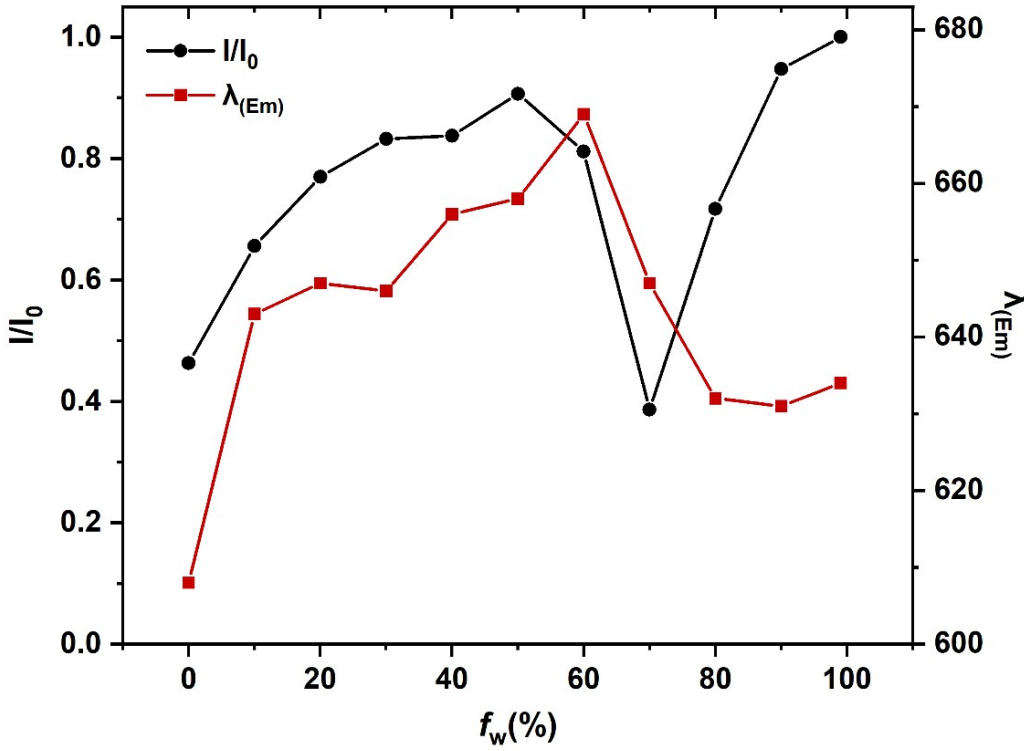

Figure S12. Plots of relative emission intensity (I/I_0, I_0 is the PL intensity of f_w=99%) and λ_{em} of **DCI-Py-2**.

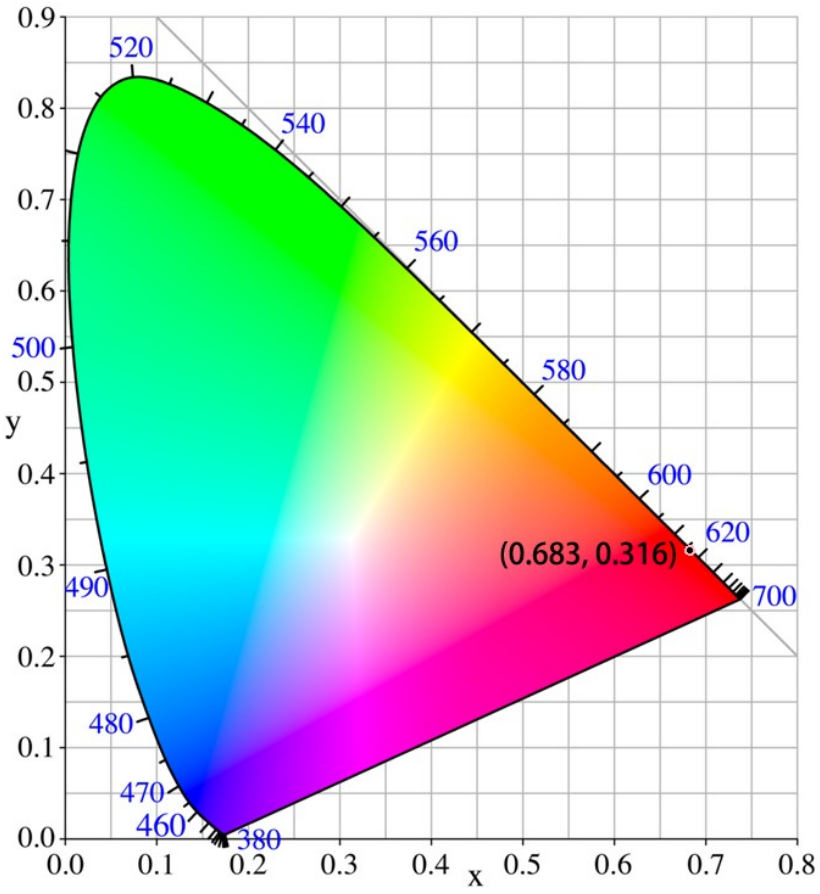

Figure S13. The CIE 1931 chromaticity diagram for luminogens **DCI-Py-1**.

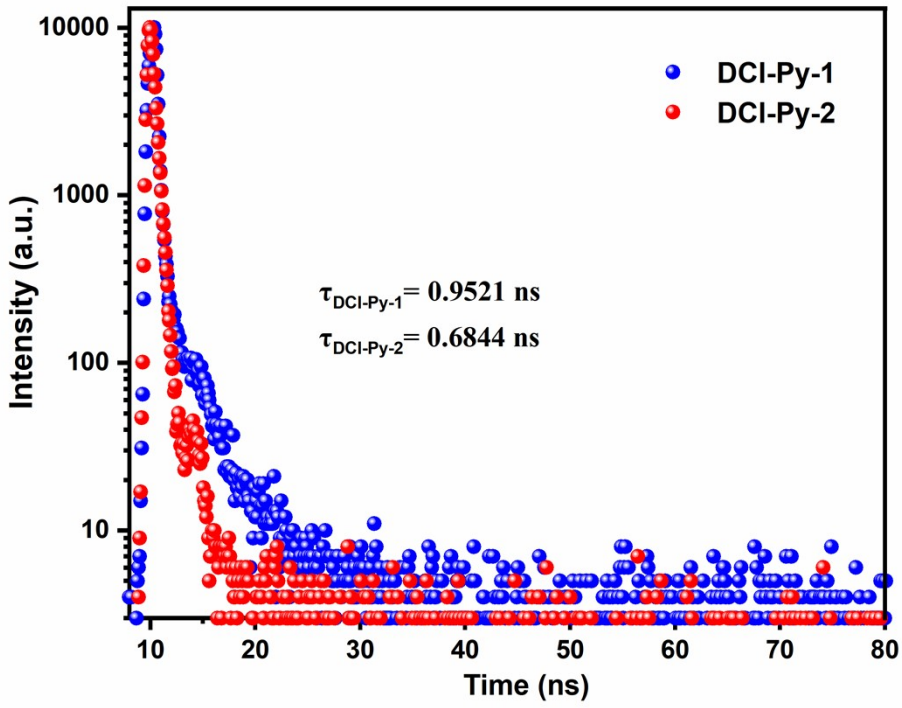

Figure S14. Fluorescence decay profiles of **DCI-Py-1** and **DCI-Py-2**.

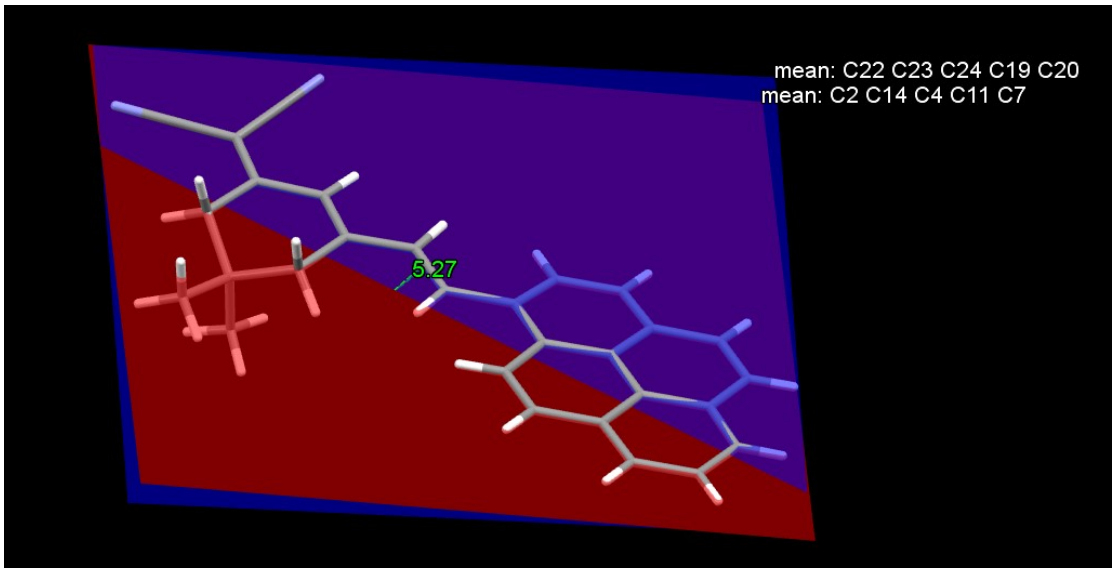

Figure S15. The dihedral angles between the pyrene core and **DCl** group in **DCI-Py-1**.

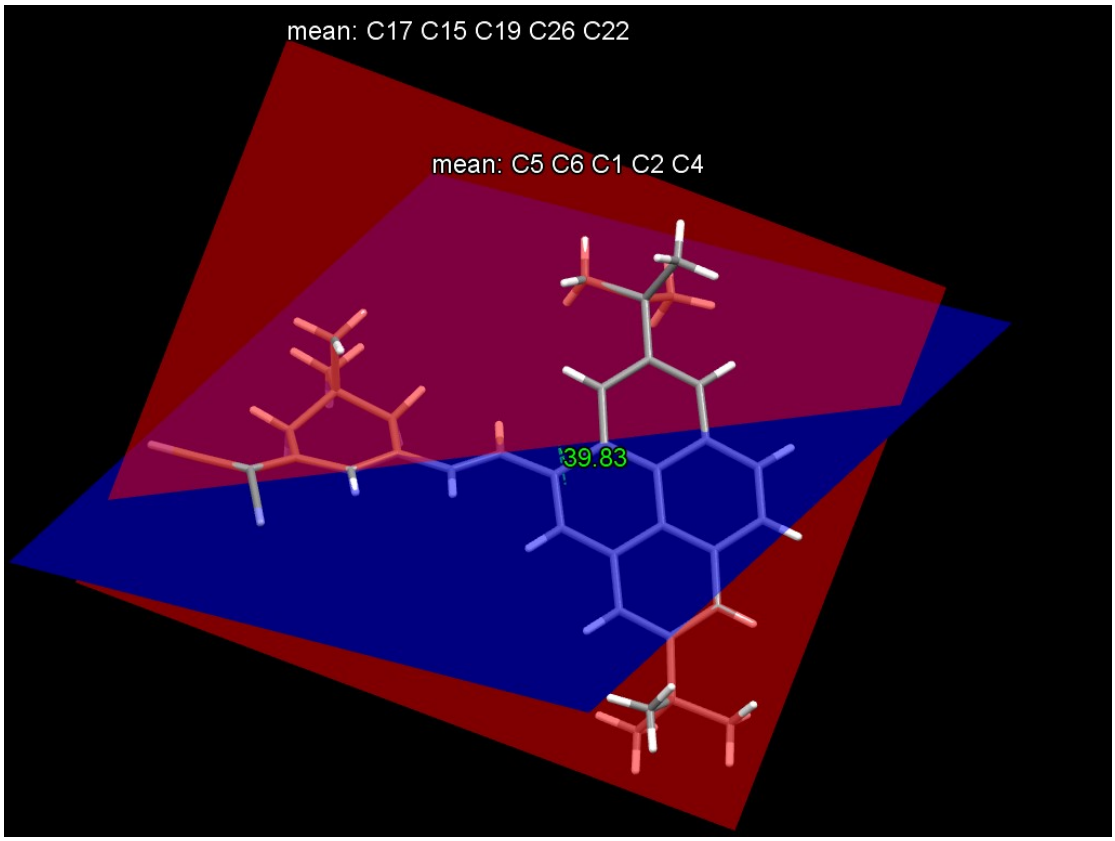

Figure S16. The dihedral angles between the pyrene core and **DCl** group in **DCI-Py-2**.